Numerical evaluation of micro- to macroscopic mechanical behavior of carbon-black-filled rubber

Tomita, Yoshihiro
Lub, Wei
Naito, Masato
Furutani, Yasuhiro

(Citation)
International Journal of Mechanical Sciences,48(2):108-116

(Issue Date)
2006-02

(Resource Type)
journal article

(Version)
Accepted Manuscript

(URL)
https://hdl.handle.net/20.500.14094/90000007

Numerical Evaluation of Micro- to Macroscopic Mechanical Behavior of Carbon-Black-Filled Rubber

Yoshihiro TOMITA*, Wei LU**, Masato NAITO*** and Yasuhiro FURUTANI*

*Graduate School of Science and Technology, Kobe University,
Rokkodai 1-1, Nada, Kobe 657-8501 Japan

**Graduate School of Engineering, Osaka Prefecture University,
Gakuen 1-1, Sakai, Osaka 599-8231 Japan

***SRI R&D Ltd., Tutui 2-1-1, Chuo, Kobe 651-0071 Japan

We investigate the characteristic deformation behavior of rubber with carbon black (CB) filler. The deformation behaviors of a plane strain rubber unit cell containing CB fillers under monotonic and cyclic strain are investigated by computational simulation with a nonaffine molecular chain network model. The results reveal the substantial enhancement of the resistance of the rubber to macroscopic deformation, which is caused by the marked orientation hardening due to the highly localized deformation in the rubber. The disentanglement of the molecular chain during the deformation of rubber results in the magnification of the hysteresis loss, i.e., the Mullins effect, occurring in stress-stretch curves under cyclic deformation processes. The increase in volume fraction and in aggregation of the distribution of CB substantially raises the resistance of the rubber to deformation and hysteresis loss. The effect of the heterogeneous distribution of the initial average number of segments of molecular chains on the hysteresis loss has been clarified.

1. Introduction

It is well known that the blending of particulate fillers such as CB as depicted in Figs.1 (a) and (b) induces a remarkable change in the mechanical properties of rubber[1]. Figure 1(c) shows the typical stress-stretch relations of CB-filled/unfilled rubbers. The hysteresis loss, i.e., the Mullins

effect [2], is seen during the loading and unloading processes for unfilled rubber. The Mullins effect for CB-filled rubber is marked compared with that of unfilled rubber, which is closely related to the ultimate properties of filled rubber[1]. Consequently, several mechanisms for the enhancement of the ultimate properties of filled rubber have been suggested[3,4]. Here, we focus our attention on the evaluation of the enhancement of deformation resistance and hysteresis loss caused by filling CB to rubber.

The constitutive equation for rubber exhibiting the Mullins effect during the loading and unloading process is established by employing a nonaffine molecular-chain network model[5], which was originally developed for the orientation hardening of amorphous polymers and may account for the change in the entanglement situation for the physical linkages during the deformation processes. Meanwhile, although the distribution of CB is somewhat aggregated to random, we assume that this distribution is periodic and establish a unit cell model composed of rubber and heterogeneous CB particles. The same constitutive equation established for rubber and the linear elastic constitutive equation are employed for rubber and CB, respectively, without introduction of additional material parameters. The computational simulations employing these constitutive equations and unit cell models of rubber containing CB clarify the mechanisms of enhancement of deformation resistance and hysteresis loss, and the effect of volume fraction and distribution patterns of CB, and the heterogeneity of the initial average number of segments of molecular chains of rubber on these characteristics. The computationally predicted results and experimental results are compared to evaluate the adequacy of the present simulation.

2. BASIC EQUATIONS

2.1 Constitutive Equations

To duplicate the experimentally observed characteristic features of the rubber, as shown in Fig.2, the microstructure of rubber is assumed to consist of long molecular chains which are randomly

distributed in space. A single chain, which consists of several segments containing monomers, is defined by two linkages which are assumed to be chemically or physically entangled points of molecular chains. The physical links are, in general, not permanent and may change depending on deformation. On the other hand, chemical links are permanent and preserve the entanglement situation. Figure 3(a) indicates a schematic illustration of a molecular chain network in the initial and deformed situations. The physical links may suffer breakdown during the thermodynamical process. Molecular dynamics simulation also suggests a change in the entanglement situation as depicted in Fig.3 (b). The decrease in the number of entangled points due to deformation causes an increase in the average number of segments N in a single chain, enhanced extensibility, and a reduction in the stiffness of the material, i.e., softening, which play a very important role in the manifestation of the hysteresis of cyclic deformation behavior of rubber[6]. To account for the change in the number of entangled points, namely, in the number of segments N, depending on the temperature change and deformation during the orientation hardening process of amorphous polymers, a nonaffine molecular chain network theory was developed [5] in which the number of entangled points is expressed as suitable function of temperature and an appropriately defined measure of deformation.

The complete constitutive equation for the rubber exhibiting the Mullins effect is derived on the basis of the nonaffine molecular-chain network theory[5]. It is easily adapted to an affine molecular chain network theory in order to account for the change in the entanglement situation depending on deformation and temperature change. Several affine molecular-chain network models have been proposed and employed for the evaluation of the deformation behaviors of rubber and amorphous polymer. Here we employ the eight-chain model [7]. The principal stress σ_i and principal stretch λ_i relations become

$$\left.\begin{aligned} \sigma_i &= \frac{1}{3} C^R \sqrt{N} \frac{\lambda_i^2 - \lambda_c^2}{\lambda_c} L^{-1}\left(\frac{\lambda_c}{\sqrt{N}}\right) - p\,, \\ L(x) &= \coth x - \frac{1}{x}\,, \quad \lambda_c^2 = \frac{1}{3}(\lambda_1^2 + \lambda_2^2 + \lambda_3^2)\,, \end{aligned}\right\} \qquad \textbf{(1)}$$

where $C^R = nk_BT$ is a constant, n is the number of chains per unit volume, k_B is Boltzmann's constant, L is the Langevin function, and p is an indeterminate hydorstatic pressure.

After some algebra[8], the rate-type expression of constitutive equation (1), which relates the rate of Kirchhoff stress $\dot{S}_{ij}$ to strain rate $\dot{\varepsilon}_{kl}$ becomes

$$\dot{S}_{ij} = L_{ijkl}\dot{\varepsilon}_{kl} - P'_{ij}, \quad L_{ijkl} = R_{ijkl} - F_{ijkl}, \quad P'_{ij} = \dot{p}\delta_{ij} \tag{2}$$

$$\left.\begin{aligned} R_{ijkl} &= \frac{1}{3}C^R\sqrt{N}\left\{\left(\frac{\xi_c}{\sqrt{N}} - \frac{\beta_c}{\lambda_c}\right)\frac{B_{ij}B_{kl}}{B_{mm}} + \frac{\beta_c}{\lambda_c}\left(\delta_{ik}B_{jl} + B_{ik}\delta_{jl}\right)\right\}, \\ F_{ijkl} &= \frac{1}{2}\left(\sigma_{ik}\delta_{jl} + \sigma_{jl}\delta_{ik} + \sigma_{il}\delta_{jk} + \sigma_{jk}\delta_{il}\right), \\ \xi_c &= \frac{d}{dx}\mathcal{L}^{-1}(x)\Big|_{x=\frac{\lambda_c}{\sqrt{N}}} = \frac{\beta_c^2}{1-\beta_c^2\operatorname{csch}^2\beta_c}, \ \beta_c = \lambda_c/\sqrt{N}, \end{aligned}\right\} \tag{3}$$

where σ_{ij}, δ_{ij} and B_{ij} are the Cauchy stress tensor, Kronecker's delta and the left stretch tensor, respectively. In this investigation, we introduce the volume constant constraints through the penalty method involving a fictitious bulk modulus K. Hence, the rate of change of the pressure in Eq.(2) is expressed as $\dot{p} = -K\dot{\varepsilon}_{mm}$, with K is at each instant determined as $K = \psi \max(L_{ijkl})$, with a sufficiently large number of ψ.

To account for the change in the number of entangled points, namely, in the number of segments N, depending on the deformation during the orientation hardening process of rubber, we adopted the nonaffine molecular chain network theory [5], where the number of entangled points depends on the suitable measure of the deformation and temperature. Here, we employ the simplest version of the nonaffine molecular-chain network model[5] to accommodate the change in the number of segments N depending on stretch λ_c, as

$$N(\lambda_c) = N_0 + f(\lambda_c), \quad Nn = \text{constant}, \tag{4}$$

where N_0 is the initial average number of segments in a single chain, $f(\lambda_c)$ is a polynomial which suitably expresses the experimental results, and we employ the quartic expression of λ_c. We obtain the nonaffine generalization of Eqs.(1) to (3) by substituting N with $N(\lambda_c)$ of Eq.(4).

2.2 Homogenization Method

So far we have restricted our attention to the unfilled rubber. With regard to the CB-filled rubber, the volume fraction, morphology and distribution patterns substantially affect the mechanical characteristics of the rubber. Here, although the distribution of CB is somewhat random, we assume a periodic distribution and discuss the essential features of the effect of filling CB in the rubber on the mechanical characteristics. To correlate the microscopic scale deformation to the macroscopic scale deformation, we employ the homogenization method.

Consider the two-dimensional (2D) problem shown in Fig.4, with domain Ω and boundary S subjected to surface force P_i on S_t and prescribed velocity on S_u. The body is formed by the spatial repetition of a base cell Y made of different materials. Assuming that the base cell is very small, of order η compared with the dimensions of the entire body, the global coordinate is x_i for the entire body and the local coordinate is y_i related to the single base cell, then $y_i = x_i / \eta$. Similar to the assumption used in the case of linear elastic materials[9], the velocity v_i is presumed to be expressed as an asymptotic expansion with respect to parameter η [10].

$$v_i(x,y) = v_i^0(x) + \eta v_i^1(x,y) + \eta^2 v_i^2(x,y) + \ldots\ldots \tag{5}$$

where $v_i^0(x)$ is the microscopically uniform part of velocity, whereas $v_i^1(x,y), v_i^2(x,y), \ldots$ are Y-periodic and local perturbations due to the presence of heterogeneities in the unit cell. In this research, we consider the first terms $v_i^0(x), v_i^1(x,y)$ in Eq.(5) only. The velocity gradient $v_{i,j}$ and strain rate $\dot{\varepsilon}_{ij}$ are expressed as

$$v_{i,j} = \frac{\partial v_i}{\partial x_j} + \frac{1}{\eta}\frac{\partial v_i}{\partial y_j}, \quad \dot{\varepsilon}_{ij} = \frac{1}{2}\left(v_{i,j} + v_{j,i}\right). \tag{6}$$

Substituting the velocity v_i into Eq.(6), we have the expression of strain rate

$$\left.\begin{aligned}
&\dot{\varepsilon}_{ij}(x,y)=\eta^{-1}\dot{\varepsilon}^0_{ij}+\eta^0\left\{\dot{E}^0_{ij}+\dot{\varepsilon}^1_{ij}\right\}+\eta^1\dot{E}^1_{ij} \\
&\dot{E}^k_{ij}=\frac{1}{2}\left(\frac{\partial v^k_i}{\partial x_j}+\frac{\partial v^k_j}{\partial x_i}\right),\ \dot{\varepsilon}^k_{ij}=\frac{1}{2}\left(\frac{\partial v^k_i}{\partial y_j}+\frac{\partial v^k_j}{\partial y_i}\right)
\end{aligned}\right\} \qquad \textbf{(7)}$$

Introducing thus obtained velocity, velocity gradient and strain rate into the virtual work principle[11,12] with the constitutive equation (Eq.(2)) and rearranging at the same order η, we arrive at the virtual work principle for a macroscopic body:

$$\int_\Omega\left[L^H_{ijkl}\dot{E}^0_{kl}-P^H_{ij}+\sigma^H_{ij}+\tau^H_{ijkl}\frac{\partial v^0_k}{\partial x_l}\right]\frac{\partial\delta v_i}{\partial x_j}d\Omega=\int_{S_t}\dot{P}_i\delta v_i dS \qquad (8)$$

$$\left.\begin{aligned}
L^H_{ijkl}&=\frac{1}{|Y|}\int_Y\left[L_{ijkl}-L_{ijpq}\frac{1}{2}\left(\frac{\partial\chi^{kl}_p}{\partial y_q}+\frac{\partial\chi^{kl}_q}{\partial y_p}\right)\right]dY \\
P^H_{ij}&=\frac{1}{|Y|}\int_Y\left[P'_{ij}-L_{ijkl}\frac{1}{2}\left(\frac{\partial\phi_k}{\partial y_l}+\frac{\partial\phi_l}{\partial y_k}\right)\right]dY, \\
\sigma^H_{ij}&=\frac{1}{|Y|}\int_Y\sigma_{mj}\frac{\partial\phi_i}{\partial y_m}dY, \\
\tau^H_{ijkl}&=\frac{1}{|Y|}\int_Y\left[\sigma_{lj}\delta_{ki}-\sigma_{mj}\frac{\partial\chi^{kl}_i}{\partial y_m}\right]dY
\end{aligned}\right\} \qquad (9)$$

$$\dot{\varepsilon}^0_{ij}=\dot{E}^0_{ij}-\frac{1}{2}\left(\frac{\partial\chi^{kl}_i}{\partial y_j}+\frac{\partial\chi^{kl}_j}{\partial y_i}\right)\dot{E}^0_{kl}+\frac{1}{2}\left(\frac{\partial\phi_i}{\partial y_j}+\frac{\partial\phi_j}{\partial y_i}\right) \qquad (10)$$

$$\dot{S}^0_{ij}=L_{ijkl}\dot{\varepsilon}^0_{kl}-P'_{ij} \qquad (11)$$

In Eq.(9) $|Y|$ indicates the area of the unit cell shown in Fig.4.

Equations (8), (9) and (10), (11) are the governing equations for the macroscopic and microscopic scales, respectively. The notations χ^{kl}_p and ϕ_k are characteristic functions defined in the unit cell, which satisfy the Y periodicity and are determined by the following equations.

$$\int_Y\left[L_{ijpq}\frac{1}{2}\left(\frac{\partial\chi^{kl}_p}{\partial y_q}+\frac{\partial\chi^{kl}_q}{\partial y_p}\right)+\sigma_{qj}\delta_{pi}\frac{\partial\chi^{kl}_p}{\partial y_q}\right]\frac{\partial\delta v_i}{\partial y_j}dY=\int_Y\left(L_{ijkl}+\sigma_{lj}\delta_{ki}\right)\frac{\partial\delta v_i}{\partial y_j}dY \qquad (12)$$

$$\int_Y \left[L_{ijkl} \frac{1}{2}\left(\frac{\partial \phi_k}{\partial y_l} + \frac{\partial \phi_l}{\partial y_k} \right) + \sigma_{mj} \frac{\partial \phi_i}{\partial y_m} \right] \frac{\partial \delta v_i}{\partial y_j} dY = \int_Y P'_{ij} \frac{\partial \delta v_i}{\partial y_j} dY \tag{13}$$

Thus, characteristic functions χ_p^{kl} and ϕ_k for the unit cell depend solely on the material characteristics and configuration of the microstructure of the unit cell, which are, in turn, obtained without interacting stress and strain of the macroscale. On the other hand, the macroscopic equilibrium given by Eq. (8) can be solved independently because the macroscopic characteristic functions indicated in Eq. (9) are identified through Eqs. (12) and (13). The homogenized material characteristics indicated by Eq. (9) reflect the volume fraction, size and distribution of second-phase-particle-dependent onset and propagation of the shear band in the unit cell. Once the average stress rate is estimated, different types of stress rates can be obtained using the same transformation rule on the microscale [13]. Equation (8) can be applied to solve the general boundary value problems for the materials with periodic microstructures under macroscopically nonuniform deformation. In the present investigation, we use Eq.(8) for clarification of the deformation behavior of a unit cell under macroscopically uniform deformation.

By the way, the relationship between $v_i^1(x,y)$, $\chi_i^{kl}(x,y)$ and $\psi_i(x,y)$ can be expressed by $v_i^1(x,y) = -\chi_i^{kl}(x,y)\dot{E}_{kl}^0(x) + \psi_i(x,y)$. The detailed derivation of this relationship can be found in [9, 10].

3. COMPUTATIONAL MODEL

The mechanical characteristics of CB-filled rubber are strongly dependent on the volume fraction and distribution patterns of CB. Although the distribution of CB is somewhat aggregated to random as can be seen in Figs.1 (a) and (b), we assume that such distribution is periodic. To evaluate the detailed characteristics of microscopic deformation and clarify their effect on the macroscopic mechanical characteristics of CB-filled rubber, discussions are focused on the essential feature of the

effect of volume fraction and distribution patterns of CB on the mechanical characteristics of CB-filled rubber.

Figure 5 shows the computational model in which heterogeneous CB are assumed distributed periodically. Here, the rubber obeys the constitutive equation (2) and CB obeys the linear elastic constitutive equation. As indicated in Fig. 5, in the present investigation, the heterogeneous CB are assumed to comprise of circular cylinders of radii r_1 and r_2 contained in a square unit cell. Case A corresponds to CB distributed throughout the unit cell, and Case B is the somewhat aggregated case. The homogenization method that indicated in the previous section has been employed to correlate the micro- to macroscopic deformation behavior. The boundary conditions on the macroscopic scale are that the top and bottom surfaces are shear-free with a constant displacement constraint, whereas the right and left surfaces are assumed to be stress-free. It is important to note that the constitutive models used do not have a material length scale. Thus, the only length scales in the problem are the cell dimensions, which govern the solution through the dimensionless variables r_1 / r_2 and volume fraction f_0.

Here we will discuss the effects of volume fraction f_0 and distribution patterns of CB with the size $r_1 / r_2 = 2$ on such macroscopic deformation behaviors as the average stress-strain relationship, hysteresis loss, i.e., Mullins effect[2], and on microscopic deformation behavior such as localization of deformation in rubber. For a typical unit cell, which is the microscopic element of CB-filled rubber, a macroscopically homogeneous strain is applied. The material parameters for the rubber employed are $N_0 = 4.5$, $N_a = 4.36 \times 10^{26}$ (the number of segments per unit volume), $C_0^R = n_0 k_B T = 0.394$, $n_0 = N_a / N_0$, $T_0 = 296\mathrm{K}$. For CB, elasticity modulus and Poisson's ratio are $E_c = 100\mathrm{MPa}$, $\nu_c = 0.3$ respectively. To suppress the onset of numerical instability caused by the extreme difference between the stiffness of CB and rubber, rather low stiffness for CB is introduced. It has, however, been verified that this value provides suitable results.

4. RESULTS AND DISCUSSIONS

First we discuss the deformation behavior of rubber without filling CB. Figure 6(a) indicates the stress-stretch relationship for unfilled rubber under cyclic loading. The dotted lines represent the experimental results. To reproduce the experimental results, we express the concrete form of Eq.(4) by using the fourth-order polynomial of λ_c and identify the coefficients of the equation, by the least mean squares method, for the loading process of the first cycle; the number of segments N is preserved during the unloading process. Furthermore, the number of segments N is preserved until the stretch λ_c due to the subsequent loading reaches the maximum value of previous loading processes. This implies that the stress-stretch relationship is identical to that of previous unloading processes up to the maximum stretch during the previous loading processes. The number of segments N restarts to change following Eq.(4) when stretch λ_c exceeds the maximum attained in the previous deformation. The resulting change in the number of segments N with respect to stretch λ_c is represented in Fig.6 (b). The corresponding stress-stretch relationships for cyclic deformation behavior are shown in Fig.6 (a) by solid lines, which reproduce the experimentally obtained results well. These characteristic deformation behaviors will be used to describe the rubber containing CB without introduction of additional material parameters.

Next, we will discuss the deformation behavior of CB-filled rubber. Although as indicated in Figs.1 (a) and (b), the distribution of CB is somewhat complicated and the shape of CB is spherical with heterogeneous sizes, here in this investigation, we try to clarify the main mechanism of enhancement of mechanical characteristics by means of simplified computational model indicated in the previous chapter. Figure 7 indicates the stress-stretch relationships for CB-filled rubber. For the purpose of comparison, the gray lines indicate the stress-stretch relationship for unfilled rubber under cyclic loading. The solid lines indicate the stress-stretch relations for CB-filled rubber in which rubber obeys the constitutive equation expressed by the gray lines. The marked increase in the resistance to deformation in the loading processes and the hysteresis loss for the CB-filled rubber

reproduce the experimentally obtained results well. Figure 8 indicates the strain distribution at six different stages of deformation during the loading and unloading stages. Small but recognizable differences between the same deformations in the loading and unloading stages is attributable to the Mullins effect. This suggests the mechanism of enhancement of the resistance and softening in CB-filled rubber. That is, the local concentration of the deformation due to the existence of CB causes a high stretching which results in a high orientation hardening and deformation induced softening. Therefore, the resistance to deformation and the hysteresia loss for CB-filled rubber are markedly increased as compared with those for unfilled rubber.

Next, the problems associated with the effects of the volume fraction and distribution patterns of CB, and the heterogeneity of the number of segments N on the micro- to macroscopic deformation behavior of CB-filled rubber are clarified by employing the computational model presented in the previous section. Three cyclic deformations up to the maximum average stretches of 1.1, 1.3 and 1.5 for the 1st, 2nd and 3rd cycles, respectively, are simulated.

Figure 9(a) shows the typical stress-stretch relationships for unfilled rubber and CB-filled rubber for cases A and B in Fig.5. Figure 9(b) shows the effect of the volume fraction of CB f_0 on the stress-stretch relationships. CB-filled rubber exhibits a markedly high deformation resistance compared with unfilled rubber. The aggregated distribution of CB, in case B, contributes to the further increase in deformation resistance. The resistance to deformation rises with an increase in the volume fraction of CB f_0. Figure 10 shows the distributions of rotation θ, stretch λ_c and tensile stress σ_{22} for cases A and B with the average stretch of 1.5. The concentrated deformation connecting the CB causes high stretching accompanied by locally large rotation in the area surrounding high stretching. The orientation hardening of rubber develops in the highly stretched area where the resistance to deformation rises and the stress attains a high value. On the other hand, in the highly rotated area, deformation is mainly absorbed by rotation and orientation hardening is suppressed, which limits the stress to a low value. The localized deformation connecting large

particles is much stronger. Therefore, in addition to the distance between the particles, the heterogeneity of the particles also affects the deformation resistance. The increase in the volume fraction of CB reduces the particle spacing, which facilitates the emergence of localized deformation connecting the particles and a high resistance to deformation. Thus, an additional increase in deformation resistance is expected upon filling the rubber with CB.

Furthermore, as indicated above, the higher concentration of the deformation causes locally high stretching in rubber, which promotes a change in the number of segments N. As a result, this contributes to the manifestation of hysteresis loss in the cyclic stress-stretch relationships. Figure 11(a) indicates the hysteresis loss for the 1st, 2nd and 3rd cycles for unfilled rubber and CB-filled rubber with patterns A and B. The hysteresis loss is defined by the difference in area under the stress-stretch curves between a loading cycle and a susequent unloading cycle. That is, $\Delta\phi = (\Delta W_H / W_L) \times 100$, where ΔW_H is the area of hysteresis loss and W_L is the area under the stress-stretch curve for the loading process. Hysteresis loss $\Delta\phi$ increases with the increases in the average stretching and the aggregation of CB. Furthermore, Fig. 11(b) depicts the effect of the volume fraction of CB on hysteresis loss for three cycles. The results suggest that the effect of the volume fraction of CB on hysteresis loss is substantial and is amplified with the increase in the number of cycles, namely, with the increase in the amount of stretch in the present loading processes. These effects are attributable to the softening caused by the change in the number of segments N due to the increase in the amount of stretch.

Finally, the effect of heterogeneous distributions of the initial average number of segments N_0 on the Mullins effect has been explored. Three normal distribution cases, as indicated in Fig.12 (a), are considered, in which the mean value, $\overline{N}_0$, is equal to 4.5, 4.5 and 9.0 and the variation, $N_0^{\max} - N_0^{\min}$, is equal to 1.5, 0.3 and 1.5 for cases 1, 2 and 3, respectively. The distribution of the initial average number of segments N_0 is specified such that, depending on the total number of

finite elements in a unit cell, a specific value of N_0 is allocated to a square element. Figures 12(b) and (c) indicate the tensile stress distributions and hysteresis loss for the corresponding cases. The increase in the heterogeneity of the initial average number of segments N_0 promotes the local stress concentration that results in the enhancement of hysteresis loss. The increase in the mean value of the initial average number of segments N_0 yields a high extendibility that drives the relaxation of the local stress concentration and reduces the hysteresis loss.

The results obtained partially clarify the essential physical enhancement mechanisms of deformation resistance and hysteresis loss, namely., the Mullins effect, for rubber filled with CB with different distribution patterns and volume fractions. The effect of the heterogeneous distribution of the average number of segments of molecular chains on the hysteresis loss has been clarified. These results describe the experimentally obtained evidence well, however, the problems associated with the time-dependent nature of the deformation behavior of the rubber[14-17] and the interface effect[18-20] between the rubber and CB should be addressed in order to refine the model.

5. Conclusion

We developed a computational model of the monotonic and cyclic deformation behavior of CB-filled rubber by means of the homogenization method and the constitutive equation accounting for the changes in the entanglement situation due to the deformation of rubber. A series of simulations has revealed the mechanisms of the enhancement of characteristic mechanical behavior of CB-filled rubber.

Initially, for unfilled rubber, the proposed model reproduces the stress-strech relations and softening, namely, the Mullins effect, that occur in the stress-stretch curves during cyclic deformation processes in the experiment well. For the case of CB-filled rubber, without any additional material parameters, the present model captures the marked increases of resistance of

deformation and the Mullins effect well, which is closely related to the orientation hardening in the rubber caused by highly localized deformation due to filling with CB. That is, the substantial enhancement of orientation hardening and promotion of the disentanglement of molecular chain of rubber results in the magnification of the hysteresis loss in stress-stretch curves under the cyclic deformation processes. Correspondingly, the increases in volume fraction and the heterogeneity of the distribution of CB substantially increases the resistance to deformation and hysteresis loss. The increase in the heterogeneity of the initial average number of segments promotes the local stress concentration that results in the enhancement of hysteresis loss. The increase in the mean value of the initial average number of segments yields the high extensibility that drives the relaxation of the local stress concentration and reduces the hysteresis loss.

All results describe the experimentally observed evidence well, however, the problems associated with the time-dependent nature of the deformation behavior of the rubber and the interface effect between the rubber and CB should be addressed in order to refine the model.

Acknowledgements

Financial support from the Ministry of Education, Culture, Sports, Science and Technology of Japan through a Grant-in-Aid for Scientific Research and a Grant-in-Aid for a JSPS Fellow is gratefully acknowledged. We are also grateful for the financial support from SRI R&D Ltd.

REFERENCE

[1] L. Mullins, Softening of rubber by deformation. Rubber Chem. Technol. **42**(1969) 339.

[2] L. Mullins, Effect of stretching on the properties of rubber. Rubber Chem. Technol. **21** (1948) 281.

[3] Y. Fukahori and W. Seki, Molecular behaviour of elastomeric materials under large deformation: 1. Re-evaluation of the Mooney-Rivlin plot. Polymer **33** (1992) 502.

[4] J.S. Bergstrom and M.C. Boyce, Mechanical behavior of particle filled elastomers. Rubber Chem. Technol. **72** (1999) 633.

[5] Y. Tomita, T. Adachi and S. Tanaka, Modelling and application of constitutive equation for glassy polymer based on nonaffine network theory. Eur. J. Mech. A/Solids **16** (1997) 475.

[6] G. Marckmann, E. Verron, L. Gornet, G. Chagnon, P. Charrier and P. Fort, A theory of network alteration for the Mullins effect. J. Mech. Phys. Solids **50** (2002) 2011.

[7] E. M. Arruda and M. C. Boyce, A three-dimensional constitutive model for large stretch behavior of rubber materials. J. Mech. Phys. Solids **41** (1993) 389.

[8] A.C. Steenbrink and E. Van der Giessen, On Cavitation, Post-Cavitation and Yield in Amorphous Polymer-Rubber Blends. J. Mech. Phys. Solids 47 (1999) 843.

[9] J. M. Guedes, and N. Kikuchi, Preprocessing and postprocessing for materials based on the homogenization method with adaptive finite element method. Compt. Meth. Appl. Mech. Engng. **83** (1990) 143.

[10] Y, Higa and Y. Tomita, Computational prediction of mechanical properties of nickel-based superalloy with gamma prime phase precipitates. Advance Materials and Modeling of Mechanical Behavior, **III**, eds. F. Ellyin and J.W. Provan, Fleming Printing Ltd., Victoria, B.C., Canada 1999.

[11] R, Hill., A general theory of uniqueness and stability in elastic-plastic solids. J. Mech. Phys. Solids, 10 , (1958) 236-249.

[12] H, Kitagawa, Y, Seguchi and Y, Tomita, An incremental theory of large strain and large displacement problems and its finite element application. Ing. Arch., 41, (1972) 213-224.

[13] N, Ohno and D, Okumura, D., On the formulation of homogenization methods of finite deformation in the updated Lagrangean form. Proc. JSME, 99.(1999) 239-240(in Japanese).

[14] A. Lion, A constitutive model for carbon black filled rubber: Experimental investigation and mathematical representation. Continuum Mech. Thermodyn. **8** (1996) 153.

[15] J. S. Bergstrom and M. C. Boyce, Constitutive modeling of the large strain time-dependent behavior of elastomers. J. Mech. Phys. Solids **46** (1998) 931.

[16] J. S. Bergstrom and M. C. Boyce, Large strain time-dependent behavior of filled elastomers. Mech. Mater. **32** (2000) 627.

[17] Y. Zhang, Z. P. Huang, A model for the non-linear viscoelastic behavior of amorphous polymers. Mech. Res. Comm. **31** (2004) 195.

[18] W. Lu and Y. Tomita, Numerical evaluation of debonding behavior in carbon black-filled rubber. Proc. WCCM VI, The 2004 Sixth World Congress on Computational Mechanics (2004) CD-ROM version, Beijing, China .

[19] N.K. Esmaeili, W. Lu and Y. Tomita, Characterization of Micro- to Macroscopic Responses of Trinary Polymer-Based Composite System. Key Engineering, Vols. 274-276 (2004) 19-24.

[20] J. K. Chen, Z. P. Huang and Y. W. Mai, Constitutive Relation of Particulate-Reinforced Visco-Elastic Composite Materials with Debonded Microvoids. Acta Materialia **51** (2003) 3375.

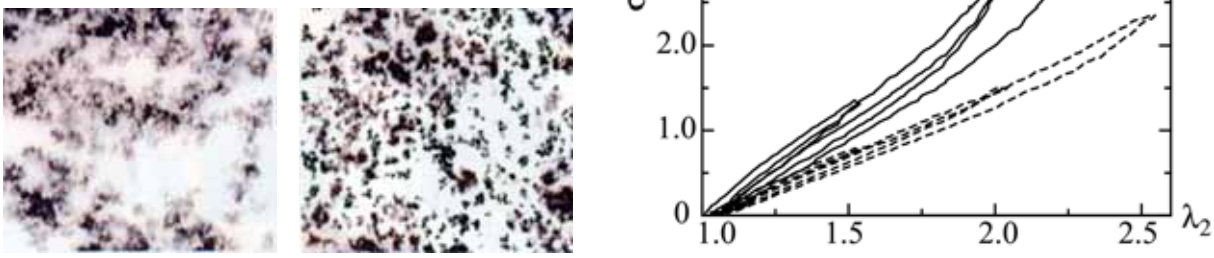

(a) Aggregated case (b) Distributed case (c) Stress-stretch relations

Figure 1 CB-filled rubber

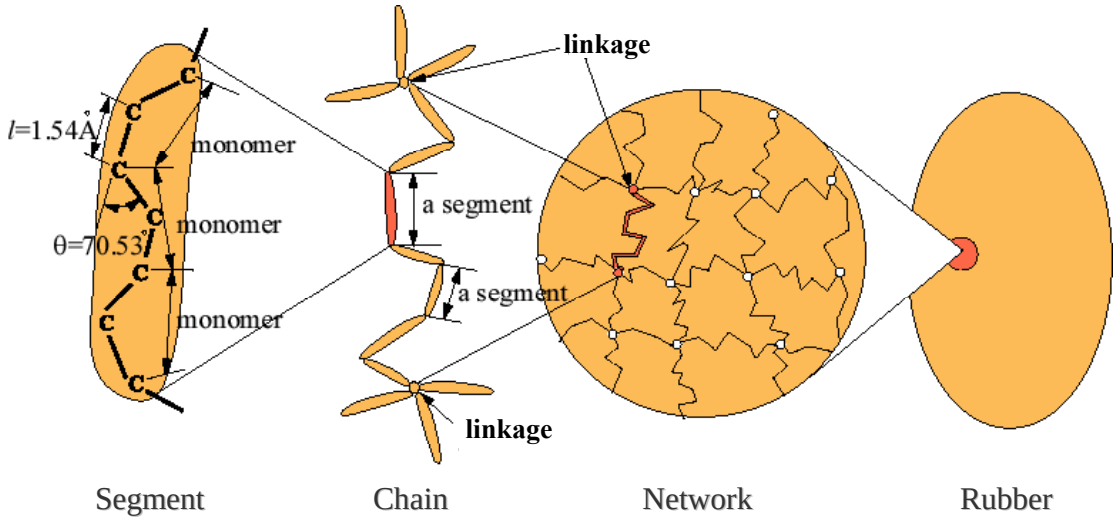

Figure 2　Hierarchy of molecular structures

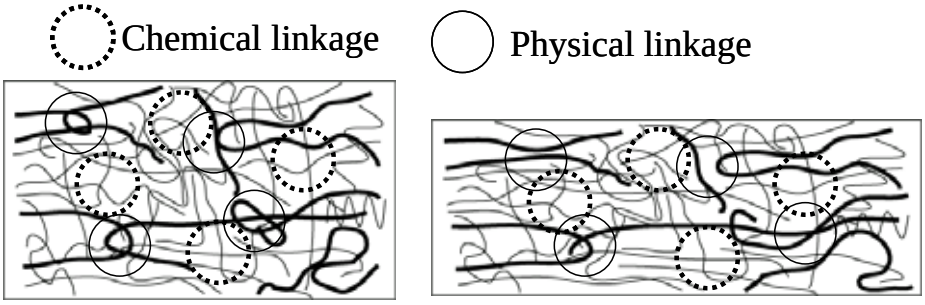

(a) initial situation (b) deformed situation

Figure 3 Deformation of molecular chain

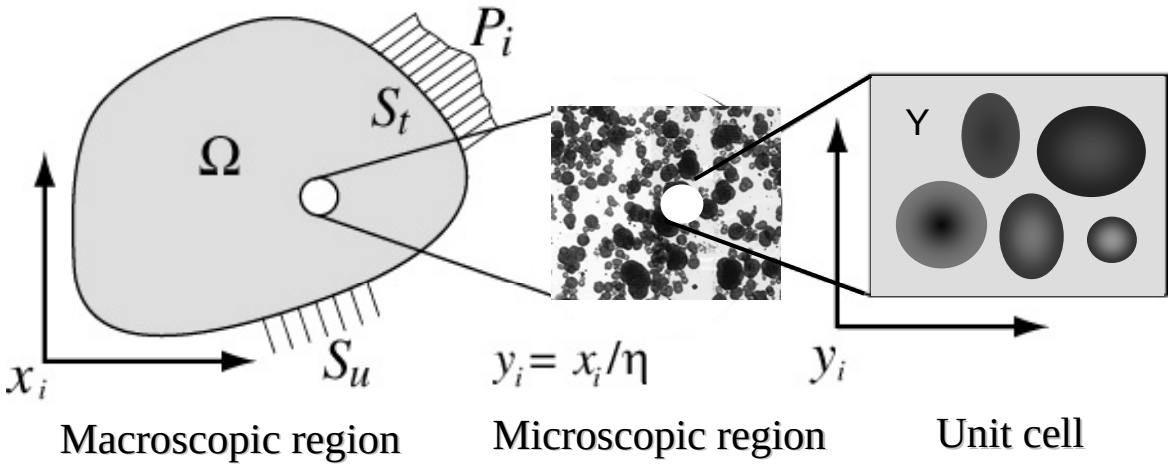

Figure 4 Explanation of homogenization method

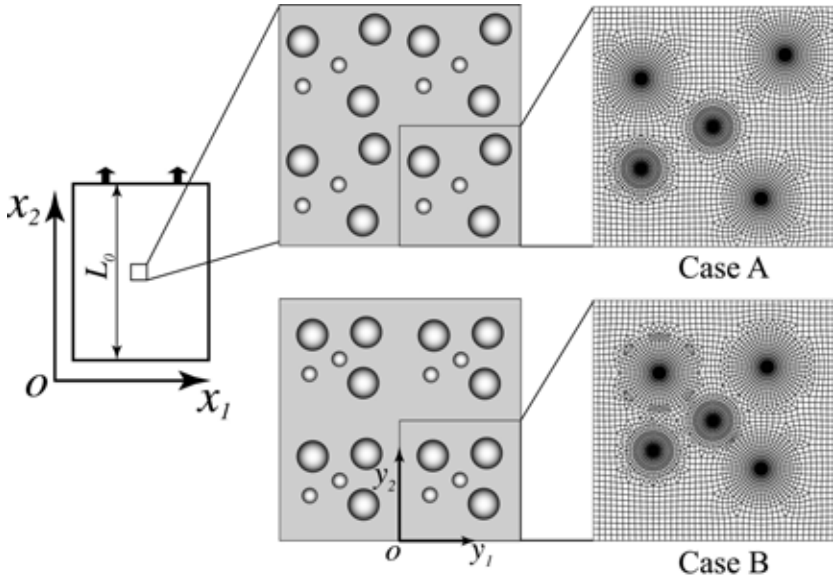

Figure 5 Simulation models of CB-filled rubber with volume fraction 20% and different radii, $r_1 / r_2 = 2$. Case A: Random distribution of carbon blacks, Case B: Aggregated distribution of CB

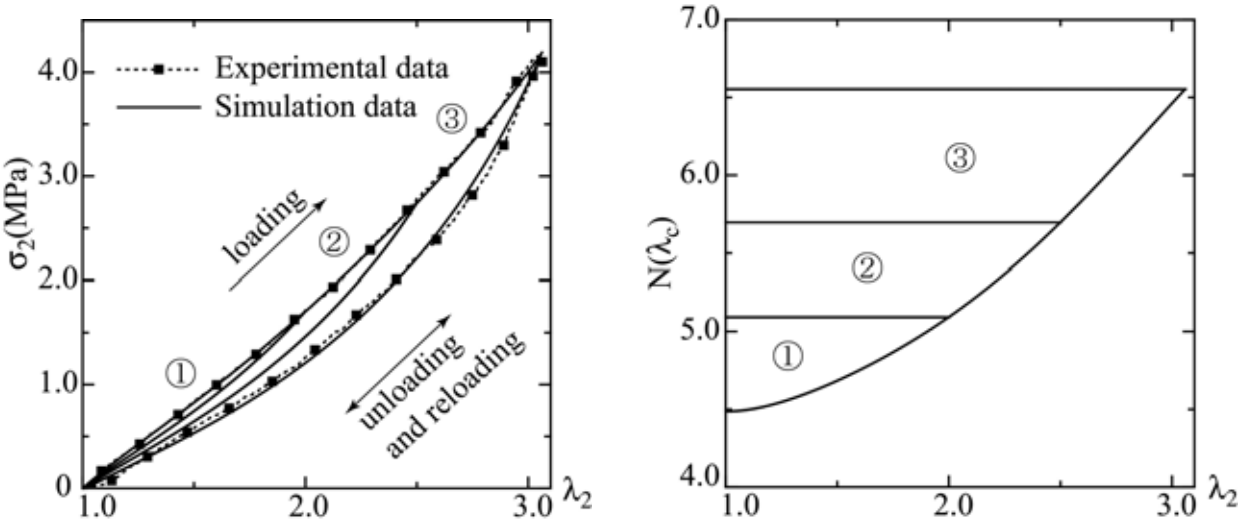

(a) Stress-stretch relationships (b) Change of the number of segments

Figure 6 Hysteresis of CB-filled rubber under cyclic loading

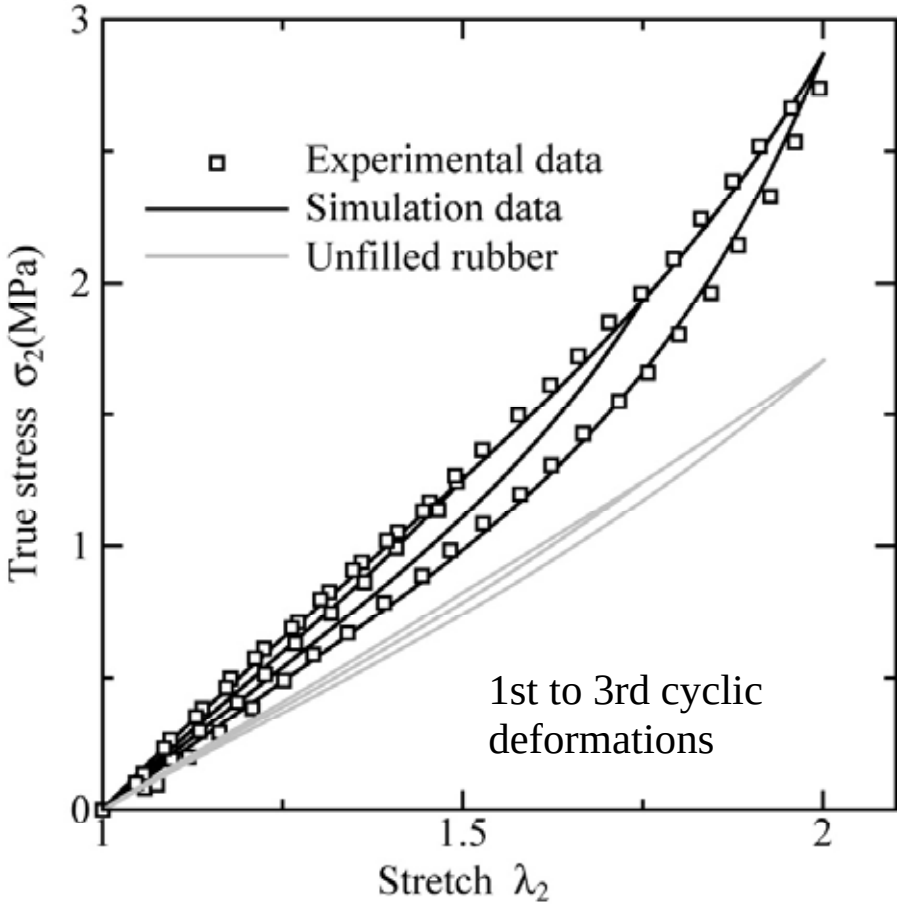

Figure 7 True stress-stretch relations for monotonic and cyclic loadings of CB-filled rubber.

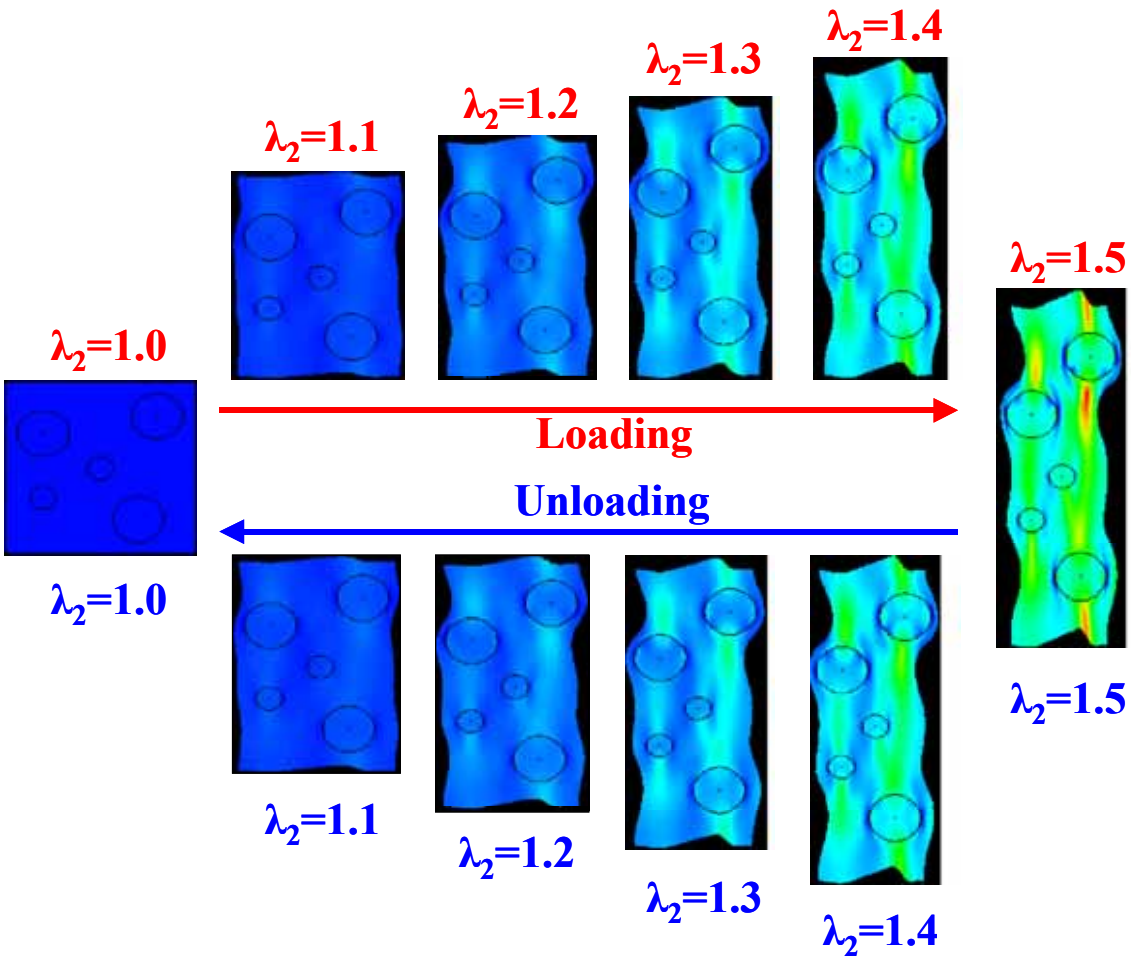

Figure 8 Snap-shot of strech distribution at different stages of deformations in loading and unloading processes

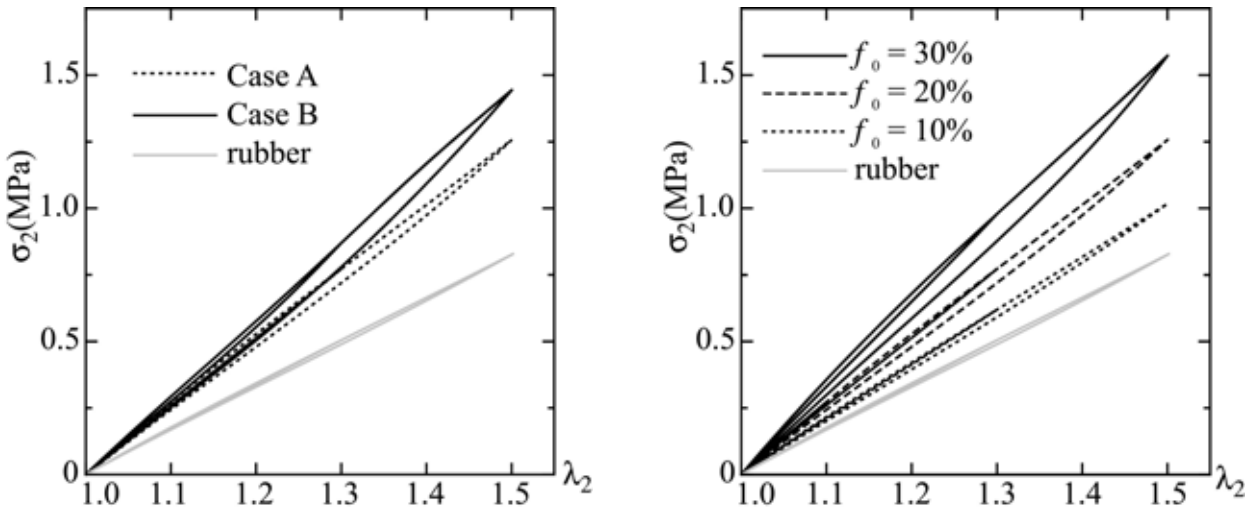

(a) Effect of distribution patterns of CB (b) Effect of volume fraction of CB

Fgure 9 Stress-stretch relationships of CB-filled rubber

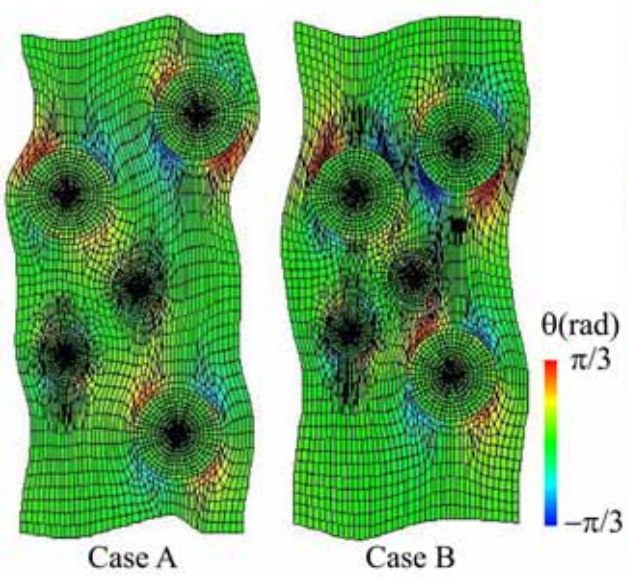

(a) Rotation θ

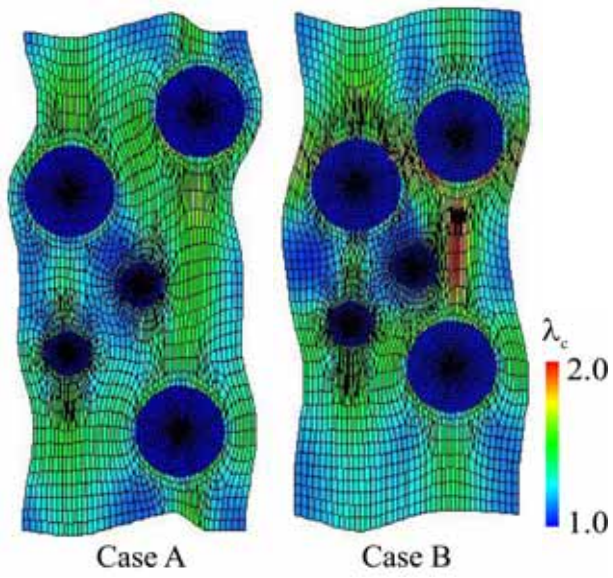

(b) Stretch λ_c

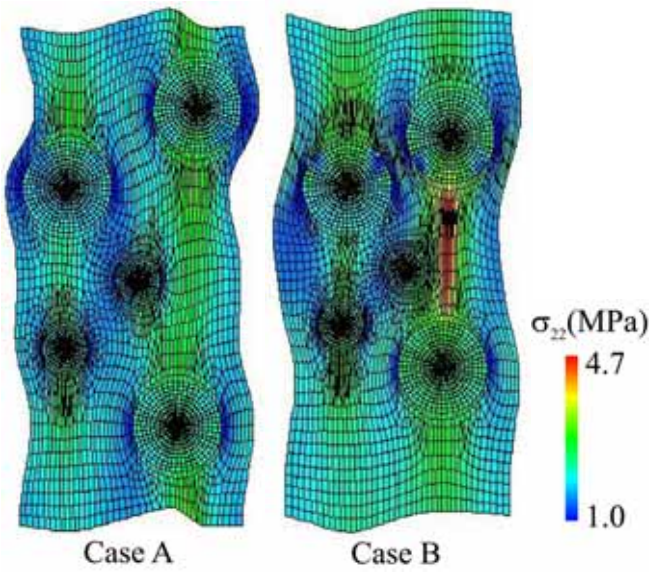

(c) Stress σ_{22}

Figure 10
Distribution of field variables

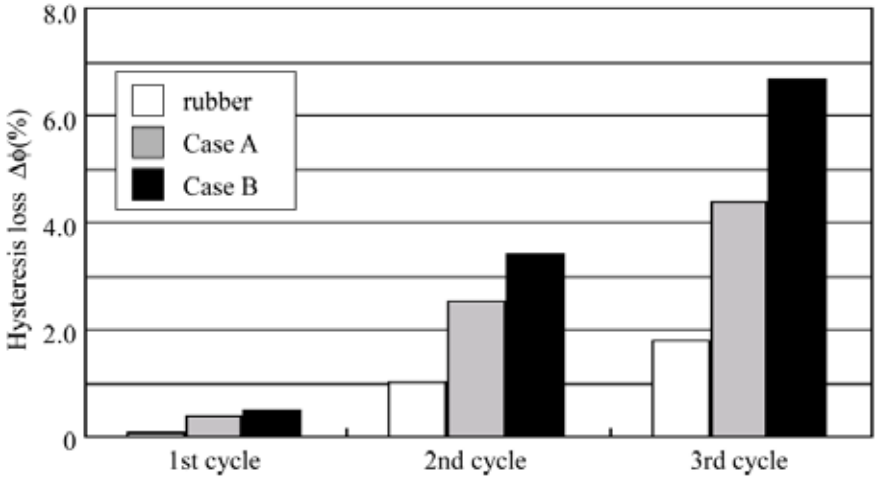

(a) Effect of distribution patterns of CB

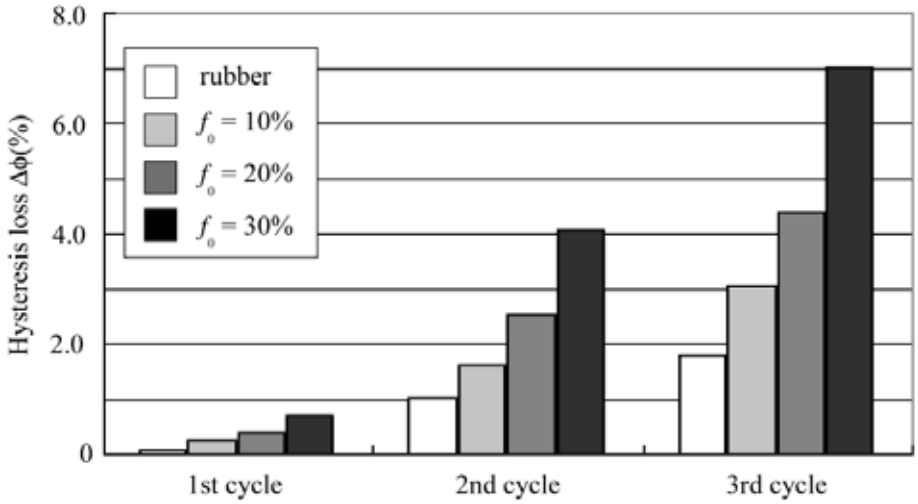

(b) Effect of distribution patterns of CB

Figure 11 Hysteresis loss

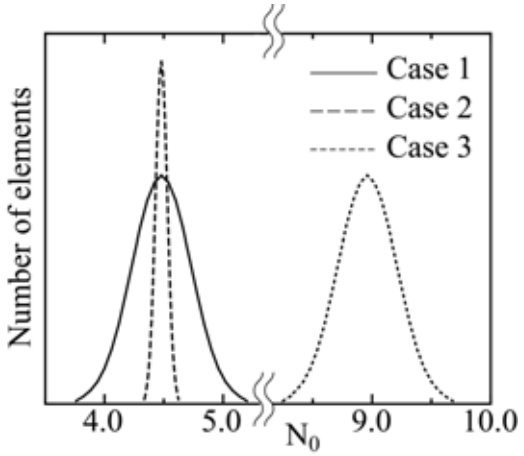

(a) Distribution of N_0

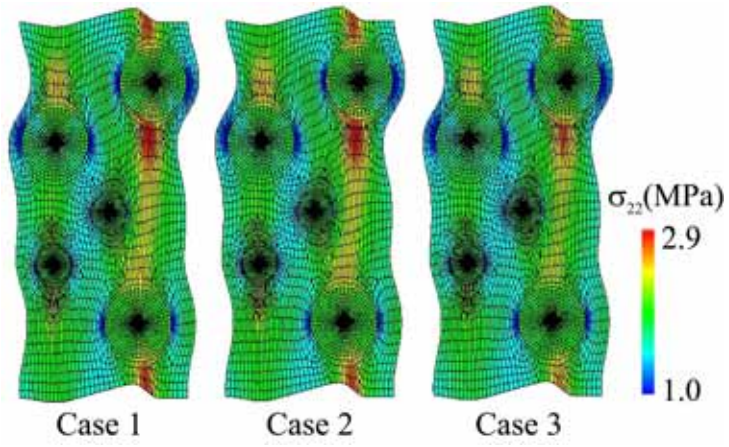

(b) Distribution of stress

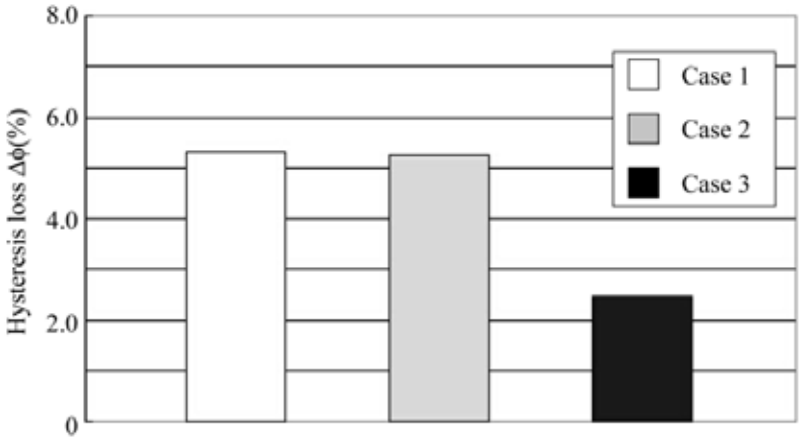

(c) Hysteresis loss

Figure 12 Effect of heterogeneous distribution of initial average number of segments N_0